Perspective: Wavefront shaping techniques for controlling multiple light scattering in biological tissues: Toward in vivo applications

Jung-Hoon Park, Zhipeng Yu, KyeoReh Lee, Puxiang Lai, and YongKeun Park

Citation: APL Photonics **3**, 100901 (2018); doi: 10.1063/1.5033917
View online: https://doi.org/10.1063/1.5033917
View Table of Contents: http://aip.scitation.org/toc/app/3/10
Published by the American Institute of Physics

Perspective: Wavefront shaping techniques for controlling multiple light scattering in biological tissues: Toward *in vivo* applications

Jung-Hoon Park,[1] Zhipeng Yu,[2] KyeoReh Lee,[3,4] Puxiang Lai,[2] and YongKeun Park[3,4,5,a]

[1]*Department of Biomedical Engineering, Ulsan National Institute of Science and Technology, Ulsan, South Korea*
[2]*Department of Biomedical Engineering, Hong Kong Polytechnic University, Hung Hom, Kowloon, Hong Kong*
[3]*Department of Physics, Korea Advanced Institute of Science and Technology (KAIST), Daejeon 34141, South Korea*
[4]*KAIST Institute for Health Science and Technology, Daejeon 34141, South Korea*
[5]*Tomocube, Inc., Daejeon 34051, South Korea*

(Received 6 April 2018; accepted 12 July 2018; published online 30 July 2018)

Multiple light scattering has been regarded as a barrier in imaging through complex media such as biological tissues. Owing to recent advances in wavefront shaping techniques, optical imaging through intact biological tissues without invasive procedures can now be used for direct experimental studies, presenting promising application opportunities in *in vivo* imaging and diagnosis. Although most of the recent proof of principle breakthroughs have been achieved in the laboratory setting with specialties in physics and engineering, we anticipate that these technologies can be translated to biological laboratories and clinical settings, which will revolutionize how we diagnose and treat a disease. To provide insight into the physical principle that enables the control of multiple light scattering in biological tissues and how recently developed techniques can improve bioimaging through thick tissues, we summarize recent progress on wavefront shaping techniques for controlling multiple light scattering in biological tissues. https://doi.org/10.1063/1.5033917

I. INTRODUCTION

Light scattering is a fundamental physical phenomenon and also plays critical roles in optical imaging. To optically visualize an object, waves scattered from individual positions in the object need to be focused via an imaging system. To achieve high contrast optical imaging, scattering (either elastic or inelastic) from a sample should be maximized, whereas scattering in the remaining path through the imaging system should be minimized. The challenges in imaging biological samples are: (i) scattering at the single cell level is very weak while (ii) scattering in a biological tissue, composed of *many* cells, is strong and exhibits multiple light scattering. To address the issue of week scattering from cells or phase objects, various interferometric techniques have been developed. Phase contrast microscopy, developed by Zernike,[1] significantly enhances the imaging contrast for biological cells by exploiting light interference. Recently, various quantitative phase imaging techniques have been developed and utilized for three-dimensional label-free imaging of live cells and tissues.[2,3] By measuring the refractive index distribution of transparent cells using the principle of interferometry or holography, quantitative phase imaging techniques achieved clear visualization of weakly scattering samples in three dimensions.[4,5] However, the issue of multiple light scattering from surrounding

[a]Author to whom correspondence should be addressed: yk.park@kaist.ac.kr

media remains a great challenge for imaging objects through biological tissues or complex media in general.

The physics of wave transport in complex media has been extensively investigated for decades, ranging from electron transport in solid states physics, to acoustic waves, and recently, to optical multiple light scattering.[6] Various theoretical and experimental methods have been developed to understand, suppress, or even utilize light transport in complex media such as biological tissues. One of the fundamental principles that enable systematic control of light scattering in complex media is that multiple light scattering in complex media that although the resultant intensity patterns exhibit highly disordered distributions, known as speckle patterns, multiple scattering itself is a deterministic process that can be precisely described using Maxwell's equations.

Recent progress in the field has focused on utilizing the deterministic nature of elastic light scattering to control multiple scattering in complex media using wavefront shaping techniques.[7,8] Measuring the optical transmission matrices of optical waves through a turbid layer enables a complete description of light transport systematically.[9] Controlling the wavefront of light impinging into complex media opens new avenues to deliver optical information through complex media and also to utilize complex media as active optical elements.[10–13] Such advances in measuring and controlling light waves in complex media could be of particular interest in medical imaging toward *in vivo* applications. Imaging and controlling light waves through intact biological tissues can have significant impacts in the field of medicine, because it may enable non-invasive diagnosis of diseases such as cancer or even treatments of cancers without involving invasive surgical procedures.

II. FOCUSING AND IMAGING IN TURBID MEDIA USING WAVEFRONT SHAPING

A. Quantification of the scattering

Light scatters when it meets interfaces having different refractive indices. In biological tissues, for instance, scattering occurs due to the intrinsic complex composition of cells and subcellular structures, exhibiting highly inhomogeneous refractive index distributions. The reason why biological tissues appear opaque is mainly due to multiple light scattering rather than light absorption. However, the term "turbid" cannot fully present the detailed characteristics of light scattering inside the turbid media, which must be explored before an appropriate scattering suppression strategy can be established.

In general, the scattering properties of the turbid media are described by the scattering mean free path l_s, the absorption mean free path l_a, and anisotropy factor g. l_s and l_a represent the mean free propagation distance before the next scattering and absorption event, respectively. The typical values of l_s and l_a in biological tissues are 10–100 μm and 1–10 cm in the near-infrared spectral region, respectively.[14] In biological tissues, $l_a \gg l_s$, suggesting that light absorption is relatively negligible compared with the scattering effects. The anisotropy factor g represents the probability of forward scattering that relates to the refractive index variation in the turbid media. Since typical biological tissues have low refractive index variation, they usually exhibit g $\cong$ 0.9, which indicates dominant forward scattering. In addition, the transport mean free path $l_s^* = l_s(1-g)^{-1}$ is also frequently introduced. l_s^* represents the mean propagation length before experiencing isotropic light scattering. In other words, a photon's trajectory changes completely after propagating a distance l_s^*, after which it moves on a random path. In many tissue imaging techniques, l_s^* has been regarded as a characteristic thickness because it is difficult for light to penetrate the medium, and its trajectory becomes completely unpredictable around this point. Typical values of l_s^* in biological tissues are 0.l–1 mm in the near-infrared spectral region. It is noteworthy that the value of l_s^* increases as the wavelength increases, which is one of the reasons why multi-photon microscopes usually have deeper penetration depths. Further information about the scattering properties in specific biological tissues can be found elsewhere.[8,14]

B. Scattering matrix

Significant amounts of multiple light scattering events in the turbid media have limited the analytic prediction of light paths and their interferences in the media. Rather, statistical ensemble

approaches have been employed, such as photon diffusion equation[15] or Monte Carlo simulations.[16] However, researchers recently recognized that the turbid media could also be considered as optical waveguides composed of numerous beam splitters. In this scheme, though it is still challenging to quantify light transport inside the medium, the distribution and trajectory can be described by linear equations using the concept of scattering matrix. Once the scattering matrix is known, the optical function of a given turbid medium can be treated systematically and the scattered field can be predicted from a given incident field, or vice versa.

This waveguide concept holds regardless of the scattering properties and thickness of the turbid media. Therefore, the scattering matrix approach has been exploited as a powerful tool to control severe multiple scattering events throughout the turbid media and the open doors for focusing and imaging through the turbid media, as realized in the pioneering work of Vellekoop and Mosk[17] and Popoff *et al.*,[18] respectively.

To investigate the scattering matrix of the turbid media, various spatial light modulators (SLMs) have been employed, including deformable mirrors (DMs), liquid crystal on silicon (LCoS) modulators, and digital micromirror devices (DMDs). LCoS SLMs are useful in dealing with a large number of independent optical modes due to its large number of independent pixels. In contrast, DMs or DMDs have the potential for fast control of light through dynamic turbid samples at the cost of reduced diffraction efficiency or pixel count. The detailed specifications, costs, and pros and cons of each type of SLMs are summarized elsewhere.[8]

Measurements of full scattering matrices are, however, still very challenging. Owing to the inherent complexity of the turbid media, there are no general relations between the elements in a matrix. Thus, a scattering matrix should be calibrated in an element-wise manner, which is a complicated and time-consuming process. For example, the scattering matrix of a turbid medium with 1×1 mm^2 slab geometry has $N^2 \cong 2 \times 10^{15}$ elements for $\lambda = 532$ nm, where $N = 2\pi A/\lambda^2$ is the number of independent optical modes (include polarizations) on each side of a turbid medium ($A = 2$ mm^2). This may take more than three weeks to measure, even with 1 GHz throughput. Fortunately, the full scattering matrix is not necessary for many practical situations; instead, subparts of the scattering matrix are utilized.

C. Focusing through biological tissues

Focusing through the turbid media is an important step for *in vivo* biomedical applications. By the definition of a scattering matrix, focused light simply corresponds to a single row vector of the scattering matrix, which is the relation between the input fields and the single point of interest. Once the row vector of a scattering matrix is acquired, according to the Cauchy–Schwarz inequality, it is possible to maximize the intensity on the point of interest by applying the complex conjugate of the row vector as an incident field.[17] The row vector information is usually retrieved by measuring a series of optical responses at the point of interest for different input fields. Various point optimization algorithms have been suggested for rapid measurements in different practical situations.[19–21]

However, the most crucial practical hurdle toward *in vivo* applications is the time-varying property of biological tissues. Owing to the extreme sensitivity of light paths to internal microstructures, the scattering matrices of biological tissues usually exhibit very short decorrelation times of <50 ms; this time is not enough to address the sufficient number of input fields for practical focus optimization.[22] To remedy this issue, fast wavefront shaping techniques using DMDs have been reported.[23]

Alternatively, phase conjugation methods have also been widely utilized for focusing through biological tissues.[24–27] This phase conjugation approach utilizes the general reciprocity of the turbid media which guarantees that every light path is bilateral. Since the optical path would not be changed under time reversal, identical scattering information can be obtained from reversed pathways. Mathematically, reciprocity can also be understood as a symmetric scattering matrix, which suggests that the measurement of a column instead of a row is also useful. Now, unlike the row vector having single output channel, the phase conjugation method increased the number of measurable channels, which makes real-time measurement possible.

In experiments, time reversal can be achieved by exchanging the roles of light emitter and absorbers. This is why the light emitter instead of the detector should be accompanied with the phase

conjugation method called "guidestar." Several guidestar recipes have been proposed utilizing the photo-acoustic effect, two-photon absorption, and particle displacements, as summarized in a previous review.[28] The details regarding the current state-of-the-art photo-acoustic guidestar technologies will be further discussed in Sec. III.

D. Imaging through biological tissues

Similar to focusing, imaging through turbidity corresponds to multiple row vectors of a scattering matrix, which is often called a transmission matrix (TM). Many existing point optimization algorithms can readily be applied to TM measurements[29,30] with multiple detectors (e.g., image sensor) instead of a point detector.

Holographic approaches had been used to imaging through a thin diffusive layer.[31–34] However, these holographic imaging methods require an interferometric system[35,36] and work only for a thin diffusive layer, which is difficult to be applied to thick biological tissues. Recently, an approach called the scattering correlation matrix was developed, which retrieves TM information from the measurement of speckle intensity patterns.[37,38] Although the TM imaging capability has been verified in various works,[18,37,39–41] there still is a barrier toward practical applications. However, more important issue toward *in vivo* imaging is how to define the spatial distribution of speckle fields through the turbid media. Unlike focusing applications that are more interested in energy delivery and integration, imaging must precisely deliver the optical responses as a function of spatial positions. Unfortunately, in many practical situations, it is difficult to define the spatial location of detectors on the other side (or inside) of the turbid media. Therefore, unless the spatial distribution of detectors is somehow predetermined, the shape of an output field always remains unknown. For example, though it is possible to focus light inside the turbid media by employing fluorescent molecules as light detectors, its spatial distribution cannot be deduced from the result.[42] Optical phase conjugation approaches suffer from the same issue, while several guidestar recipes based on additional modalities (e.g., ultrasonic wave) may provide supplementary spatial information.[43,44]

To remedy such imaging disabilities, the "memory effect" has frequently been utilized. The memory effect presents the residual correlation between the input and output fields of the turbid media for tilting or shifting operations within a limited range.[45,46] This yields huge advantages in imaging applications: (i) it enables one to deduce the adjacent row vectors without additional measurements and (ii) it provides the relative spatial offset between the "output" fields. Thus, the turbid media within the memory effect range could simply be considered as a conventional linear shift-invariant system having a rather complex point spread function.[47] Exploiting such advantages of the memory effect, various approaches have been suggested to "see through" turbidity.[48–52] Among the contributions, Bertolotti *et al.*[49] and Tang *et al.*[50] provide especially important insights to practical applications by imaging hidden fluorescent objects through the turbid media.

Nevertheless, it should be noted that the memory effect only holds within a limited range. This range is a function inversely related to the degree of scattering and the thickness of the turbid media L,[45,53] or proportional to $\lambda\sqrt{l_s^*/L}$ as recently verified.[54] According to these prior studies, biological tissues are turbid media and are good for the memory effect due to their relatively high l_s^*. Moderate scan range has also been demonstrated, even over a thickness of a few millimeters of tissue specimens that corresponds to several l_s^* in a recent report.[55] Alternatively, far-field laser speckle interferometry with two-point intensity correlation measurement was also used to image object though a turbid medium.[56,57]

Working toward *in vivo* applications, however, one should consider the short decorrelation time of live tissues. The decorrelation time of live tissues is inversely proportional to the thickness of the tissue L and is expected to decay even faster for $L > l_s^*$ due to the loss of directionality. This is one of the main reasons that current wavefront shaping techniques are more focused on "aberration correction" that originates from the uneven surface and bulk effect of biological tissues when $L \leq l_s^*$ rather than general suppression of multiple scattering. Details regarding the current state-of-the-art *in vivo* wavefront shaping technologies will be further discussed in Sec. IV.

III. GUIDEDSTAR-ASSISTED WAVEFRONT SHAPING-BASED OPTICAL FOCUSING INSIDE THICK SCATTERING MEDIA

As briefly discussed in Sec. II, wavefront shaping techniques for optical focusing at depths inside scattering media typically include two categories. These are pre-compensated wavefront shaping techniques[8,19,58–63] to counteract the phase/intensity distortions induced by multiple scatterings and time-reversed wavefront shaping techniques[24,64–69] to phase-conjugate scattered light back to the guidestar inside the scattering medium. Although the goals are identical, these two categories differ in both principle and implementation. In the former category, an SLM is used to shape the spatial phase/intensity distribution of an incident beam before it is projected onto a scattering medium. The optimum wavefront is usually obtained by an iterative algorithm[17,19,58,70] or by measuring the transmission matrix (TM) of the complex medium.[35,59,71] The implementations are usually time-consuming due to the requirement for thousands of optimization iterations and, consequentially, the refreshing of patterns on the SLM at each iteration.[70,71] The latter category, in comparison, does not involve so many iterations and hence can be inherently much faster. In this method, distorted light exiting the scattering medium is holographically recorded by using a phase conjugation mirror (PCM) that can be a photorefractive material[24,65,67] or a well-aligned digital camera-SLM module.[68,72–74] Once the phase-conjugated copy of the scattering signal beam is obtained, it is projected back into the scattering medium and converges to the point of origin. Within a complete time-reversed operation cycle, the phase pattern on the SLM needs to be refreshed only once. Optical focusing within several milliseconds has been demonstrated using this method,[75,76] opening hopes toward *in vivo* applications.

Nevertheless, to focus light at depths within a scattering medium, no matter which category of wavefront shaping is used, an internal guidestar must exist or be designed to produce a feedback signal that is proportional to the *in situ* optical flux in the region of interest (ROI). This could be an actual detector or source, such as a photodiode,[71,77] CCD camera,[17,78] and emitting fluorescence molecules.[73] However, using these probes for biomedical applications is usually not favored as creating physical access to the targeted position is typically invasive and undesired. Moreover, optical focusing enabled by these physical probes is restricted to fixed positions and cannot be freely moved within a tissue sample. To overcome these limitations, researchers have developed various internal guidestars so that diffused photons emerging or propagating through the ROI can be specifically tagged or preferentially detected.[67,79,80] Among the many guidestar options, ultrasound has been demonstrated as a good candidate as it is noninvasive, label-free, and nontoxic. Moreover, ultrasound is scattered much less than light (~1/1000) in tissues, providing an accurate pinpointing at depths. Therefore, optical focusing approaches reviewed in this section center around using ultrasonic mediation, including both active (e.g., ultrasonic modulation of light)[67,72,77,80,81] and passive (e.g., photoacoustic sensing)[59,70] forms, as the internal guidestar. The employment of ultrasound also inspires the development of other guidestars, such as optical perturbation induced by absorbing objects[82–85] and microbubble activities,[44] which will also be introduced in this section.

A. Optical focusing through pre-compensated wavefront shaping

By converting absorbed photons into heat and generating not-so-scattering ultrasonic waves, photoacoustic sensing can accurately localize a signal source in scattering media. Moreover, the photoacoustic signal strength is linearly proportional to the *in situ* optical flux within the ultrasound transducer focal region. Therefore, it can potentially serve as a nearly perfect noninvasive guidestar. The idea of photoacoustically guided wavefront shaping (PAWS) was first proposed in 2011 by Kong *et al.*,[86] which has rapidly gained attention and has been followed by several other research groups.[87–91] Using the amplitude of photoacoustic signals as feedback for optimization algorithms that control the updating of the wavefront compensation patterns on the SLM, optical energy within the ultrasonic focus gradually increases with the growth of the feedback signal. After many iterations, an optical focus can be formed out of the initial random speckle pattern. The focus diameter is spatially confined by the ultrasonic focus, and the focal intensity can be enhanced theoretically by $R \approx \pi/4(N/M)$ before and after optimization, where N is the number of independently controlled modulating elements on the SLM and M is the number of speckle grains encompassed within the

ultrasonic focal region. Thus, if one wants intense optical focusing, more independent elements on the SLM (large N) and/or a higher frequency ultrasound transducer (tighter focus, smaller M) is required. The former option, however, is restrained to a maximum pixel count of 1920×1080 with a commercial SLM,[8,60,61,71] and the latter is typically limited within 50 MHz, beyond which new challenges arise regarding transducer fabrication and acoustic attenuation in biological tissues.[92,93] Assuming a 50 MHz ultrasound transducer is employed, the acoustic focal region is typically ~50 μm, containing $\sim 4 \times 10^4$ fully developed speckle grains at an optical wavelength of 532 nm. This would lead to an enhanced focal ratio of no more than 10, even when the largest possible N value is assigned. Moreover, optimization requires more than 1×10^6 iterations for computation and phase refreshing on the modulator, which could last several hours and is very time-consuming.[59,70,71] These challenges have prevented broad application of PAWS.

The aforementioned limitations of PAWS optical focusing in spatial resolution, peak intensity enhancement, and optimization time have severely prevented PAWS optical focusing from seeing wide applications. To overcome these issues, researchers have explored nonlinearity in photoacoustic (PA) signal from different perspectives, which makes it possible for PAWS to break the acoustic diffraction limitation and obtain tighter focusing.[94] From the perspective of generating nonlinear PA signals, Lai *et al.*[70] developed a dual-pulse excitation approach that fires two identical optical pulses shortly separated in time. This would generate two PA signals with different amplitudes due to the so-called Grueneisen relaxation effect,[94] and the difference between these two linear PA signals is nonlinear. Moreover, a higher concentration of optical energy onto fewer speckle grains leads to a stronger nonlinear PA signal amplitude. Therefore, wavefront optimization based on such a nonlinear feedback signal strongly favors energy focusing toward fewer (and eventually a single) optical speckle grains rather than a relatively even distribution over all speckle grains within the ultrasonic focus. The concept has been validated in a study (Fig. 1), where many random speckle grains were initially pre-focused to the ultrasonic focal region with regular single-pulse PA signals as the feedback for PAWS ($N = 192 \times 108$ on the SLM). After that, two optical pulses separated by 40 μs were fired every 20 ms, producing nonlinear PA feedback for iterative optimization. Finally, a single speckle grain with 5–7 μm optical focus was formed around the center of the ultrasonic focus. The focal enhancement ratios from the linear and nonlinear PAWS optimization stages were about 60 and 100, respectively, suggesting a factor of 6000 improvement in the peak optical fluence before and after PAWS optimization.

Apart from the above-discussed iterative approach, ultrasonically encoded light can also be used as the internal guidestar for iterative wavefront shaping.[77] Moreover, the optimum wavefront compensation required to enable focusing can also be obtained by measuring the optical TM of the scattering medium. In the first TM implementation of wavefront shaping,[35] a camera was used to measure the optical field behind a scattering medium. The measured output matrix corresponds to specific input modes (SLM modes). If all possible input modes on the SLM are enumerated, the TM bridging the input and output modes can be extracted. With the TM being acquired, arbitrary optical focusing or delivery to any location(s) within the camera's field of view can be obtained simply by inversing and manipulating the TM. Similar to the use of PA signal as feedback in iterative wavefront shaping, photoacoustic transmission matrix wavefront shaping was also developed using linear PA signal amplitudes as the measured output corresponding to each individual input mode.[59] Focusing performance comparable with the PAWS can be obtained.

B. Optical focusing through time-reversed wavefront shaping

For time-reversed wavefront shaping, the internal guidestar must perturb the optical field originating from the region of interest, which can be holographically recorded and then phase-conjugated (often referred to as "played back"). In this regard, ultrasonic mediation has served as an encouraging noninvasive internal guidestar in a class of techniques recently developed by researchers, called time-reversed ultrasonically encoded (TRUE) optical focusing[80] (a digital version shown in Fig. 2). The whole processes can be divided into two steps: the phase recording step and the playback step. In the phase recording step, the sample beam is modulated by the ultrasound with a frequency shift of f_{us}, interfering with a reference beam that is shifted with the same frequency by an acousto-optic modulator (AOM). The interference pattern is recorded by the camera, as shown in Fig. 2(a).

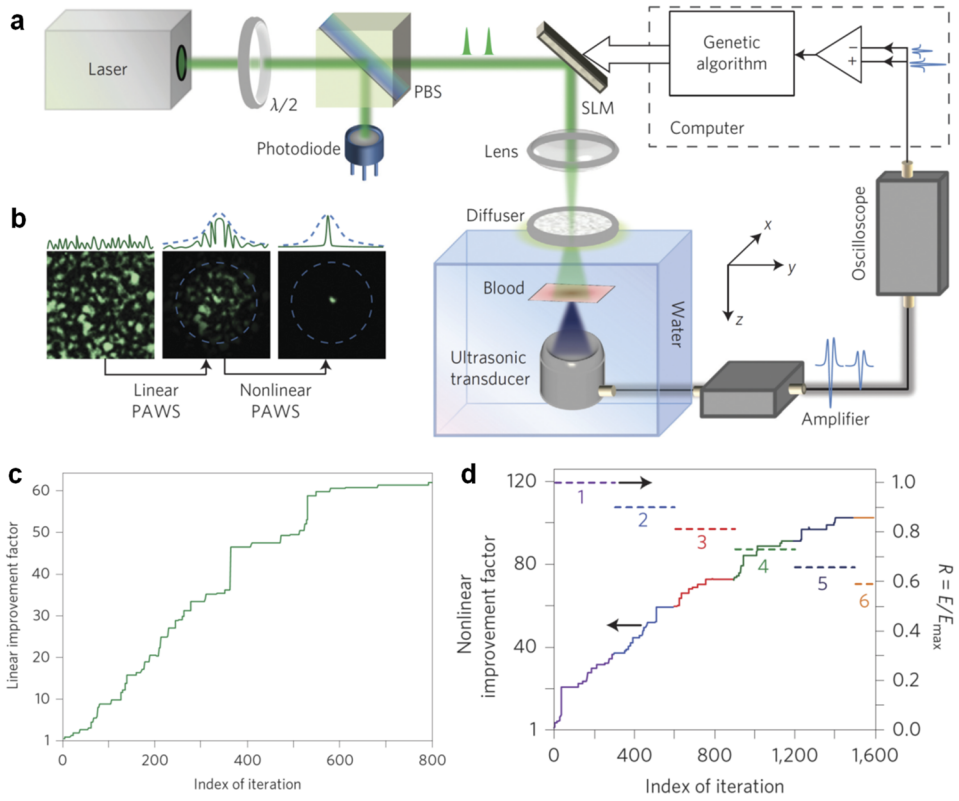

FIG. 1. (a) A pilot two-stage PAWS optimization setup. λ/2: half-wave plate; PBS: polarizing beam splitter; SLM: LCoS-type spatial light modulator. (b) Illustration of optimization outcomes with linear and nonlinear PAWS, respectively. The blue dashed circle outlines the ultrasonic focal region. [(c) and (d)] Linear and nonlinear improvement factor (defined as the ratio of the detected photoacoustic amplitudes and the initial photoacoustic amplitude) versus iteration index during two-stage optimization. Reproduced with permission from Lai *et al.*, Nat. Photonics **9**(2), 126–132 (2015). Copyright 2015 Nature Publishing Group.

In the playback step, the reference beam serves as the playback beam and is projected onto the SLM (which is conjugated to the camera and displayed with the same phase pattern calculated in the phase recording step in advance). The playback beam is then reflected into the sample and converges to the original ultrasound focal spot [Fig. 2(b)]. To measure the point spread function and to quantify the resolution of the focusing system, a fluorescent quantum dot-filled polyacrylamide (PAA) bead (<20 μm in diameter) was placed between two pieces of *ex vivo* chicken breast tissue. Figure 2(c) shows an epifluorescence image from this sample. The approximate location of the bead can be inferred based on the forward scattering nature of the biological sample. However, scattering from tissue results in very strong blurring that prohibits imaging at high resolution. In contrast, Fig. 2(d) shows a well-resolved image of the bead illuminated with time-reversed light. As the bead is smaller than the ultrasound focus, the imaged size of the bead effectively estimates the three-dimensional resolution of the focusing system. The profiles in each dimension were fit by Gaussian point spread functions with widths of 36 and 56 μm (full width at half maximum), respectively, in the lateral plane perpendicular to the light propagation axis.

As in linear PAWS, the focusing resolution of TRUE is acoustic diffraction-limited. Later on, two improved implementations, time reversal of variance-encoded (TROVE) light[43] and time-reversal ultrasound microbubble-encoded (TRUME) light,[44] were proposed to break this limit and yield sub-acoustic or even optical diffraction-limited focusing. Moreover, inspired by the employment of ultrasound, time-reversed adapted-perturbation (TRAP) optical focusing was developed using optical perturbation caused by moving absorbers[82,83] as the internal guidestar. Compared with the ultrasonic modulation-based schemes, the major advantage of TRAP focusing is the perturbation efficiency. In addition, ultrasound lacks specificity; for targeted light delivery (such as in

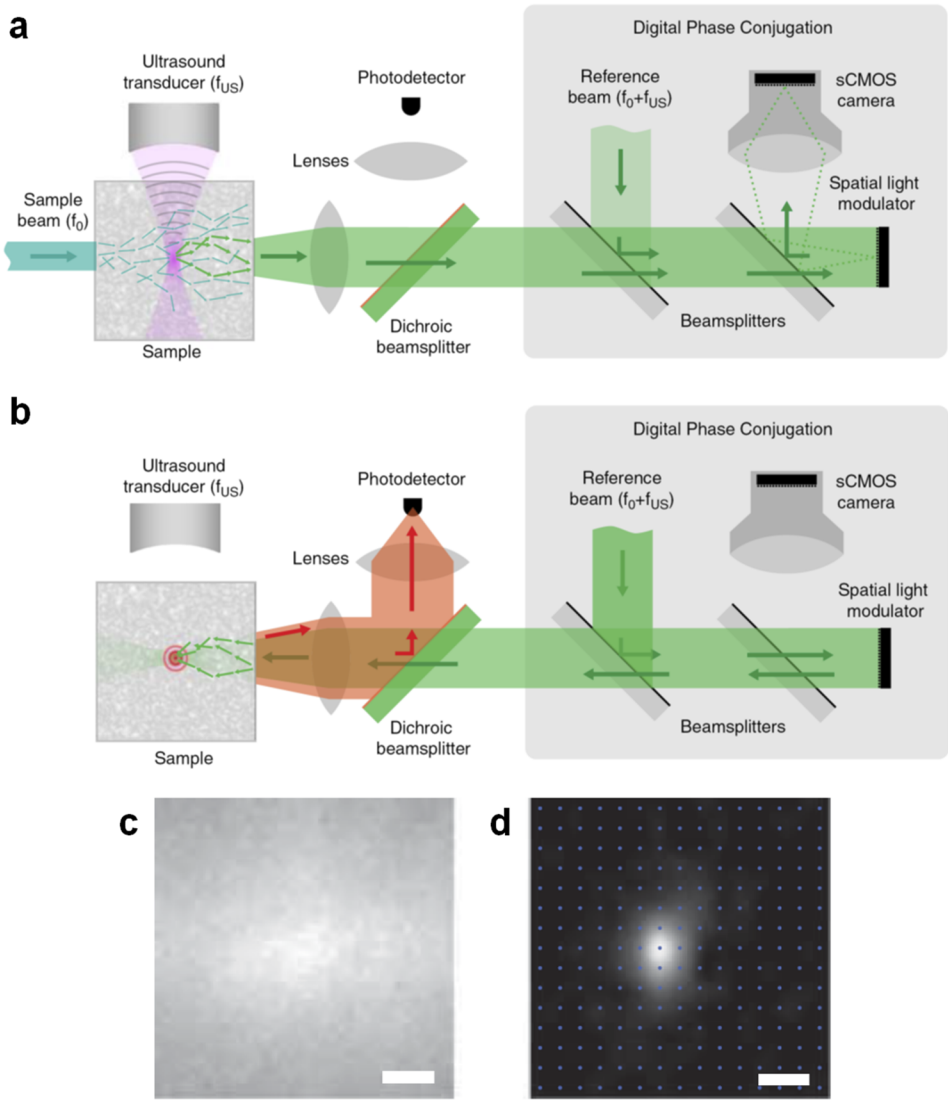

FIG. 2. The principle of TRUE, using ultrasonically encoded diffused light as the internal guidestar for optical phase conjugation. (a) Recording step. (b) Playback step. (c) Epifluorescence image of the sample in the *xy* plane without TRUE, showing very strong blurring due to tissue scattering. (d) Fluorescence image obtained by raster scanning the ultrasound transducer in *x* and *y*, with fluorescence excited by the time-reversed light. Reproduced with permission from Wang *et al.*, Nat. Commun. **3**, 928 (2012). Copyright 2012 Nature Publishing Group.

photodynamic therapy), an image must be acquired before the region of interest is determined. As a result, ultrasonic modulation-based focusing concentrates light only at the ultrasonic focal region, whereas TRAP can simultaneously enhance energy deposition onto the perturbed target in the entire field of view. To overcome the lack of remote control for perturbation movement in TRAP focusing, time-reversed magnetically controlled perturbation (TRMCP) optical focusing was recently developed using an implanted guided magnetic particle to produce the guidestar signal.[84,85]

C. Wavefront shaping-enabled deep-tissue applications

The capability of generating high-resolution wavefront shaping optical focusing with the aid of internal guidestars in deep scattering media can potentially benefit many biomedical applications in terms of resolution, signal-to-noise ratio, sensitivity, efficiency, and penetration depth of current biomedical imaging implementations. For example, enhanced fluorescence imaging in scattering

media has been thoroughly investigated.[72,80,95] By spectrally rejecting the low-frequency components in the detected PA signals, PAWS can lead to single speckle-scale optical focusing.[91] By scanning such optical focusing, one can obtain super-resolution photoacoustic imaging of a sweat bee wing, which can reveal rich information on the wing structure. The application also goes beyond imaging. Most recently, researchers have manifested optogenetic modulation of neural activity in an 800-μm-thick acute mouse brain slices using TRUE focusing.[96]

D. Discussion

As reviewed, the progress of technical development in the field is encouraging and more studies have focused on moving the techniques toward preclinical and clinical settings. Nevertheless, there is still a long way ahead with a few key challenges.

For pre-compensated wavefront shaping, the biggest challenge at the moment is the focusing speed. Taking nonlinear PAWS focusing,[70] for example, it took multiple hours in the pilot study to complete wavefront optimization and obtain an intense single speckle-scale optical focus. Such time-consuming drawback is mainly due to the inherent requirement of many (typically thousands or even tens of thousands) iterations for signal measurement, data transfer, algorithm computation, and phase pattern refreshing on the wavefront modulator. An improvement roadmap, mainly including the use of a faster wavefront modulator, onboard data acquisition, parallel processing, and more efficient optimization algorithm, has been detailed in the literature[61] and will not be reiterated here. For time-reversed wavefront shaping, the optical focusing optimization speed can already be completed within several milliseconds,[67,75,76] and the biggest obstacles toward *in vivo* are probably guidestar perturbation or modulation efficiency[83] and the complexity of the system.[74] Owing to the former factor, the peak-to-background ratio of an optical focus within scattering media is usually lower than 500, which quite often is insufficient for many applications.[80,82,83] Moreover, analog optical phase conjugation-based schemes result in limited attainable optical energy in time-reversed light, since holographic playback simultaneously erases the hologram recorded in the photorefractive material.[72,80] Digital schemes do not possess such energy limitations but are throttled largely due to some demanding requirements in system design, alignment (especially the pixel-to-pixel match between the digital camera and the SLM), operation, maintenance, and the maximum pixel number N supported by existing wavefront controllers in the market.[95]

Therefore, on the one hand, researchers have to wait for the advancement of the limiting hardware listed above, such as wavefront modulator and photorefractive material. On the other hand, there are also needs to develop new internal guidestars that produce efficient optical perturbation or emit feedback signals and are scalable in resolution, remotely controllable, biocompatible, and photostable. Last but not the least, internal guidestar-assisted wavefront shaping focusing within scattering media is still in its infancy, and it requires contributions from many experts in different disciplines. Unfortunately, not many groups around the world are partaking at this time due to various reasons. As researchers already in this field, we have the obligation to promote it, make it known to a more general audience, and attract more teams with diverse backgrounds. With these improvements, this technique has the potential to break the fundamental limitation of efficient optical focusing and controllable delivery at depths in living biological tissues, which could potentially bring a revolutionary advancement to many biomedical optical applications.

IV. WAVEFRONT SHAPING FOR *IN VIVO* IMAGING

A. Adaptive optics in astronomy in comparison with *in vivo* imaging

Since aberrations and multiple scattering are general phenomena that occur whenever light passes through any source of refractive index inhomogeneity, wavefront shaping has found use in many different areas of research which rely on the detection of waves. Regarding light-based imaging, wavefront shaping, also widely known as adaptive optics (AO), was originally developed in the field of astronomy[97] (its history is quite long, with the first proposal[98] made in 1953). This is related to a simple fact, namely, that the thick volume of atmosphere covering the earth can never be removed for us to gaze freely at the distant stars. Since we cannot remove the atmosphere, the only remaining option is to

reduce its effects to a minimum. The extreme case can be achieved by building space-bound telescopes that can avoid the deleterious effects of the atmosphere altogether, albeit at extremely high costs and system complexity. Because of pragmatic reasons, all telescopes cannot be sent out to space; so, the majority of large aperture telescopes are built on high mountaintops in desert areas, which exhibit a relatively dry and stable atmosphere. However, even in such cases, diffraction-limited imaging of astronomical objects requires dynamic aberration correction induced by remaining atmospheric turbulence.

In bioimaging, or microscopy in general, initial developments to peak into tissues were driven in another direction. There are probably two reasons for this trend. First, in contrast to the atmosphere, removing overlaying layers of tissue is a relatively easy task. Therefore, most biological microscopes (even today) are designed to work on cultured cells or thin tissue slices. In other words, cells of interest can still be observed at high resolution without dealing with cumbersome overlaying tissues. Second, for aberrations to become an issue, imaging must be performed inside a thick tissue, which is the same as saying that 3-dimensional imaging must be possible. In this respect, multiphoton microscopy and optical coherence tomography (OCT), which are currently the major workhorses for deep tissue imaging, were only first invented in 1990 and 1991, respectively. Therefore, we can see that the bioimaging community lacked a platform that could greatly benefit from wavefront shaping until relatively recently. However, since interactions between each cell and its environment are widely understood to be critical in understanding life, high-resolution *in vivo* imaging is high on the list of prospective future microscopy developments. This can easily be seen in the research field as applications of adaptive optics (or wavefront shaping) in microscopy have been steadily increasing since the late 1990s.[99–101]

One might expect that due to the large gap between the accumulated knowledge and the history between the two fields, direct application of adaptive optics from astronomy to microscopy will be a trivial task. However, it turns out that although the physical principles are the same, the relative parameters that we face are quite different. For example, considering the time domain, adaptive optics in astronomy requires fast correction of atmospheric turbulence, typically in the order of 1–10 ms. This means that a real-time feedback loop between the wavefront sensor and the wavefront modulator has to be made. This limits current developments to be mostly focused on Shack-Hartmann wavefront sensor (SHWS)-based measurements and MEMS-based wavefront modulators for correction. On the other hand, considering the spatial domain, aberrations accumulated through the atmosphere are usually much weaker than when light passes through a thick tissue. This is very fortunate as Shack-Hartmann wavefront sensors can give a reliable wavefront measurement, and the limited number of MEMS mirrors are still adequate to recover diffraction-limited resolution in astronomy. In contrast, depending on the type and thickness of the tissue, the magnitude of aberrations and the decorrelation time vary widely for bioimaging. Therefore, developments in various types of wavefront sensing and modulation schemes are currently being developed for different realms of bioimaging, as we will discuss below.

B. Direct wavefront sensing-based *in vivo* imaging

For wavefront shaping to work, the first step is to measure the aberrated wavefront. Initial wavefront shaping developments in bioimaging also used SHWS-based wavefront measurements since there is no need to construct a reference arm as in conventional holographic imaging systems. By measuring the shift of the focused light per microlens in a SHWS, the local slope of the wavefront can be easily measured, even for temporally incoherent light sources. However, since the number of lenses in the microlens array limits resolution, this approach is constrained to measuring low-order aberrations. The approach, however, has still produced a large impact on high-resolution imaging of transparent systems, such as in retinal imaging or imaging of transparent embryos.

A major advantage of SHWS-based wavefront sensing is that it is compatible with various contrast sources, including backscattered light and fluorescence.[102] For systems where most of the light is scattered from a concentrated layer such as the retina, it has been shown that simply placing the SHWS at the pupil plane of the microscope and measuring the backscattered light can effectively measure aberrations due to imperfections in the human lens and cornea. The first demonstration of an adaptive optics scanning laser ophthalmoscope[103] [Figs. 3(a) and 3(b)] also showed that descanning of

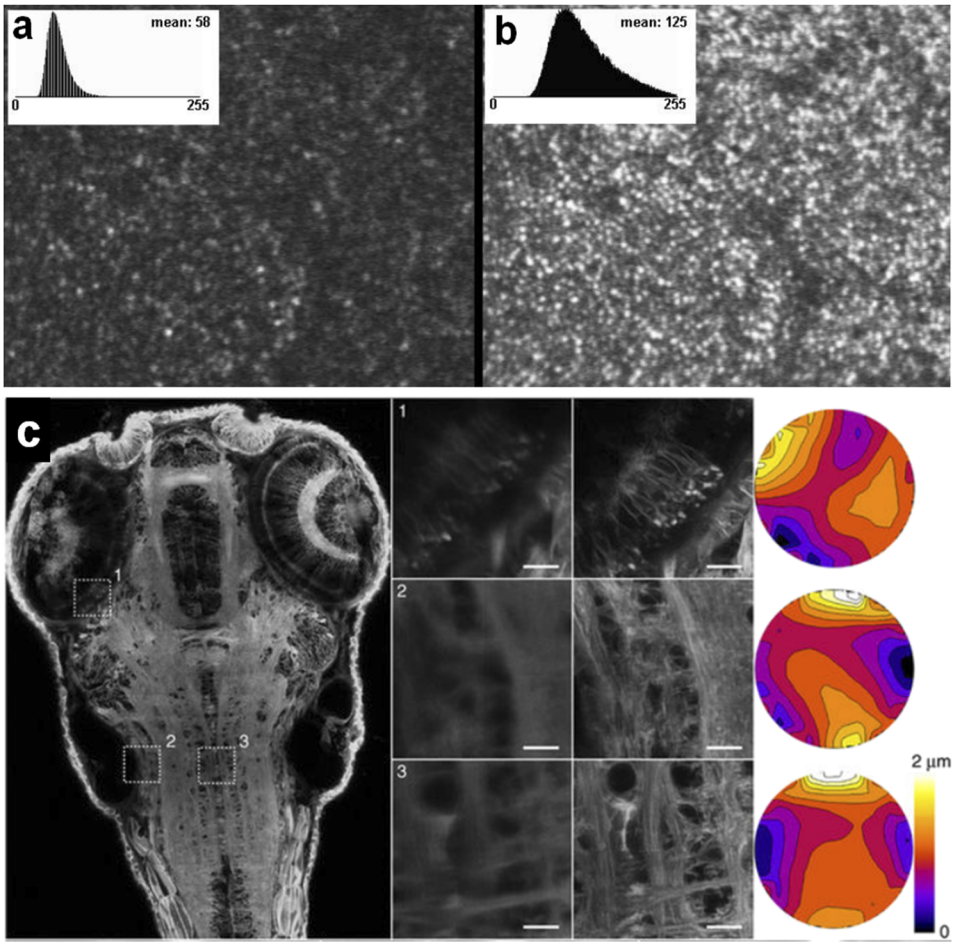

FIG. 3. Direct wavefront sensing-based AO microscopy. (a) Retina imaged with conventional scanning laser ophthalmoscopy. (b) Same area imaged with AO scanning laser ophthalmoscopy. The RMS wavefront error was reduced from 0.55 to 0.10 μm. (c) Image of living zebrafish using AO two-photon excitation fluorescence microscopy at 150 μm depth. Three numbered regions show magnified images before (left) and after (right) AO correction. The different corrections that were sequentially measured and corrected in different regions are shown on the right. The scale bar is 10 μm. Reproduced with permission from Roorda *et al.*, Opt. Express **10**(9), 405–412 (2002). Copyright 2002 Optical Society of America and 2014 Nature Publishing Group.

scattered light in confocal microscopy results in a stationary wavefront signal upon the sensor plane, enabling adaptive optics to be applied to laser scanning microscopy systems. Also, this geometry showed multiple advantages that speckle due to the coherent light sources can be averaged out by scanning and that averaging of the measured wavefront across different areas of the retina to extend the effective corrected area could also be easily achieved.[104] In other cases, where the structure is hard to define in terms of backscattering, fluorescent beads can be injected at a depth of interest to use as the guidestar for wavefront measurements using a SHWS [Fig. 3(c)], although this approach would require invasive surgery.

Due to the characteristics of the SHWS, applications for *in vivo* imaging using SHWSs for aberration measurements have been mostly focused on ophthalmology.[105,106] In this case, although OCT is usually the method of choice for retinal imaging as it provides depth-resolved imaging, AO-OCT utilizing conventional SHWSs does not have the depth resolution required for aberration measurement. This is certainly an important limitation. But fortunately, for ophthalmology, the largest source of aberrations comes from the objective lens of the imaging system, which is the cornea and lens for humans. In such cases, a depth-invariant aberration can be assumed for retinal imaging. For imaging a thick scattering tissue, on the other hand, a depth-resolved aberration measurement is required, which can be achieved by adapting conventional strategies for holography which must provide a reference

arm to measure interferometric signals. For depth-selective aberration measurements, coherence gating has been the method of choice,[107,108] and the correction obtained using coherence gating has also been shown to be effective for multiphoton excitation in an OCT-multiphoton multimodal microscope.[109]

C. Indirect wavefront sensing-based *in vivo* imaging

Direct wavefront sensing has a clear advantage that can be seen even from its name; it directly measures the aberrated wavefront in a single measurement. Therefore, if the measurement is accurate, the only remaining issue is to correct for the aberration. However, the performance of SHWSs is limited to low-order aberrations. This is because each microlens performs a wavefront measurement over a finite extended area. If there is a linear phase ramp across this area, the microlens will perform perfectly in measuring this phase ramp. However, if we consider a speckle field to be present across this area, the microlens will fail to measure this field. In other words, each microlens measures not a single phase ramp but a complex superposition of multiple phase ramps (plane waves with different incident angle) with random phase distributions, which results in a speckle being detected in the detector plane rather than the single shifted focus required for SHWSs to work. Since aberrations in biological tissues are typically more severe than in the atmosphere (seeing through millimeters of skin is harder than seeing through kilometers of air), conventional SHWSs fail to work in many opaque tissues.

An additional difficulty in conducting direct wavefront measurements in bioimaging is that it is not straightforward to construct a guidestar for wavefront sensing. As mentioned previously, SHWSs are not depth-selective and therefore cannot be used alone for depth-varying aberration measurements. Therefore, if SHWSs are to be used for depth-varying aberration corrections, fluorescent guidestars that do not overlap axially must be artificially placed in different layers of the sample. This would not be trivial to accomplish and also would be invasive.

To overcome such limitations, indirect wavefront sensing schemes have been developed specifically for deep imaging in opaque tissues where multiple scattering becomes important. Indirect wavefront sensing methods utilize the relation between aberrations and the Strehl ratio to deduce the aberrating wavefront.[110,111] Defining the maximum intensity of the focus as 1 in a non-aberrated system, the Strehl ratio describes the ratio between the maximum intensity of the focus inside the actual operating environment compared with the theoretical maximum with no aberrations. The maximum value is therefore 1 and the Strehl ratio describes relatively how severe the optical system is aberrated. By rule of thumb, a Strehl ratio of 0.8 is typically considered as an acceptable value that yields diffraction-limited resolution. Since a non-aberrated system refers to the case where a plane wave is incident on the back-pupil plane of the objective lens, the goal of all wavefront shaping systems is to correct the wavefront so that the combination of the incident light field and the distortion due to the biological tissue exactly cancel each other. Therefore, the efficiency of wavefront correction is proportional to the degree of accuracy in measuring the aberrated wavefront.

The Strehl ratio for aberrated wavefronts can be approximated as $S \sim e^{-(2\pi\omega)^2} \sim 1 - (2\pi\omega)^2 + \frac{(2\pi\omega)^4}{2!} + \cdots$ for Strehl ratios as small as 0.1, where ω is the root mean squared (RMS) wavefront error.[112] We can see that the Strehl ratio will increase as the aberrations are reduced. In this approach, the aberrated wavefront is not measured directly. Rather, the measured image itself is used to define the Strehl ratio or a related image metric. For example, sequential optimization in wavefront shaping is based on the indirect approach where the intensity of focus (Strehl ratio) is used as the metric for feedback-based iterative optimization.

Similar approaches have been demonstrated in biological systems utilizing fluorescent beads that were injected into the tissue to use as a beacon to probe the dynamically changing focus intensity as a function of different wavefronts given by a spatial light modulator. Instead of using a SHWS, the fluorescence intensity emitted from a single fluorescent bead was measured in order to find the optimum phase for each input mode. The goal is to have all input modes constructively interfere on the fluorescent bead.[102] However, although this method works nicely when a single fluorescent bead is available as the beacon, this method fails to work when the single beacon is not available and aberrations are severe. For example, if there were two fluorescent beads nearby, this approach will

not guarantee that a single tight focus will be optimized. Equal intensity distributed between the two beads will have the same total fluorescent intensity when all the incident power is distributed over a single bead. Because the initial aberrations will distort the image we can measure, only the total fluorescence will be a reliable metric, which will cause this method to fail.

This limitation can be overcome by using nonlinear excitation for the feedback signal.[50,113–115] Since the nonlinear response always favors the majority of light being focused to a single fluorescent beacon, the total fluorescence intensity can be conveniently used as the feedback signal to obtain a single diffraction-limited focus. Using this approach, indirect wavefront sensing can be achieved without invasive injection of fluorescent beacons onto the sample. By simply using the fluorescence-labeled cell of interest as the beacon, a focused laser beam can be parked at a target position of the cell and indirect wavefront sensing at that position can be performed. By measuring the total multiphoton fluorescence intensity from the focused laser beam while modulating its wavefront, the wavefront that results in maximum fluorescence intensity can again be found. Here, one must take care that photobleaching does not affect the indirect wavefront measurement, which is totally dependent on the fluorescence intensity. The measurement itself can be made in a sequential or parallel manner, where the wavefront is divided into any orthogonal basis of preference. For example, the pixels of the spatial light modulator, angular spectrum, Hadamard basis, Zernike modes, etc., can be used to reconstruct the wavefront. Using the pixels as independent modes is also known as the zonal approach. Other approaches, where groups of pixels are used to define each mode, are known as modal approaches. When using modal approaches, all of the incident light can be used simultaneously for measurement, which increases the signal-to-noise ratio. When the zonal basis approach is used sequentially, a lower amount of light decreases the signal-to-noise ratio. To overcome this limitation, recent results have demonstrated that parallel measurements can be made using the zonal approach as well by using frequency multiplexing. However, the measurement time is still equivalent for both sequential and parallel measurement methods, which make indirect wavefront sensing methods slower than direct wavefront sensing by at least 2–3 orders of magnitude (depending on the number of measured modes).

Another useful approach based on nonlinear fluorescence is to use the entire image as the metric for feedback-based optimization. Instead of parking the beam at a stationary position and performing iterative phase modulation and fluorescence intensity measurement, an image can be obtained per phase modulation. This is also known as image-based adaptive optics.[116] In this case, the obtained images per phase modulation can be used to obtain wavefront corrections for the entire field of view or at arbitrary positions within the field of view.

Although nonlinear fluorescence excitation has been demonstrated to be powerful and allows the use of endogenous fluorescent cells as beacons for indirect wavefront sensing, there still are some limitations. First, some of the precious fluorescence budget has to be used during wavefront sensing, which might mean that there would not be any fluorescence left for actual imaging. Even worse, phototoxicity can kill the cell of interest. In the extreme case, unstable fluorophores might even bleach before the wavefront measurement can be completed. Second, it still relies on fluorescent probes to be distributed across the sample. This limits the delivery of aberration-corrected light only to areas near the fluorescent area. This could create limitations, for instance, when the target application is not imaging but rather sending a tight focus deep inside the tissue for phototherapeutic purposes.

To deal with such limitations, an approach that does not require any fluorescent beacon and can be used at arbitrary positions was demonstrated using backscattered light. To filter out light that has been scattered from specific depths, broadband excitation combined with coherence gating was used.[117–119] This approach is also limited as this method will not be able to measure a signal where backscattering is low, but this limitation is expected to be minor for most biological tissues. Using coherence-gated backscattered light for indirect wavefront sensing (either with zonal or modal approaches) has been shown to focus light through a 500-μm-thick brain slice[117] and was used to obtain B-scan images of a live mouse tail.[120]

D. Enlarging the corrected field of view

An additional difficulty that wavefront shaping faces in general is that turbid media are random by definition. This also applies to biological tissues. Owing to heterogeneity in the distribution of cells and their subcellular organelles, the correction for a single focus located deep inside the tissue

is not valid for another location. The area where the correction is valid is known as the isoplanatic patch, which defines the corrected field of view for a single correction. In general, the deeper one aims for a condition where the more scattering is the tissue, the smaller is the isoplanatic patch. Ironically, the easiest way to overcome this limit is to deliberately make the aberration correction less accurate. This can be accomplished by taking the wavefront measurement over an extended area so that the wavefront aberrations are averaged over the targeted range. This has been demonstrated for both direct sensing and indirect sensing approaches. Especially in the indirect sensing approach, image-based adaptive optics clearly demonstrates the trade-off between the correction efficiency and the corrected field of view. For example, if the total intensity of the entire field of view is used as the feedback metric, the aberration measurement would be averaged over the entire field of view. In this case, the correction will not be perfect due to the averaging, but it will be effective over a large imaging area. If higher correction efficiency is required, a smaller portion of the field of view can be chosen for feedback, which will result in a wavefront measurement that is more accurate for this particular area. However, it will now be more inaccurate for other parts of the field of view, thus constraining the effective field of view.

This trade-off between the corrected field of view and the correction efficiency is already well known in astronomy. Limitation in the corrected field of view is due to the three-dimensional heterogeneous distribution of the refractive index. In astronomy, the corrected field of view was extended by employing multi-conjugate adaptive optics, where the aberrations for different layers of the atmosphere were corrected for independently using multiple wavefront modulators corresponding to each layer. This was accomplished by first measuring the aberrations from different layers by using a tomographic reconstruction approach. The volume wavefront aberrations were measured from different directions using multiple wavefront sensors.[121]

However, although simulations have shown that microscopy will also benefit from multi-conjugate adaptive optics,[122–124] directly applying this approach to microscopy has proven to be difficult, despite the improvements it would provide. This is primarily because it is not straightforward to separate aberrations from different layers in highly turbid media. In all tomographic reconstruction algorithms developed to date, approximations regarding the propagation of light, such as the Born approximation, must be valid to reconstruct a high-resolution 3D volume. When multiple scattering severely scatters the light paths inside the turbid medium, this approximation is no longer valid and high-resolution tomography becomes impossible. Because of such difficulties, applications of multi-conjugate adaptive optics in microscopy have so far been limited to dual-conjugate[125] or single-conjugate[126] configurations. Dual-conjugate wavefront correction was demonstrated to be effective in retinal imaging, where two deformable mirrors were conjugated to the pupil and slightly in front of the retina, respectively. Single conjugate geometry was shown to be highly effective in situations where aberrations are highly concentrated on a single effective layer, such as the skull (Fig. 4). In this case, a deformable mirror was conjugated to the skull, which demonstrated extension of the corrected field of view by a factor of approximately 16-fold compared with the conventional adaptive optics, where the correction is performed in the Fourier plane.

Another recent approach, termed multi-pupil adaptive optics, suggested an alternative way to extend the corrected field of view.[127] Instead of dividing the aberrating volume into different layers, the aberrations that differ for different parts of the field of view were measured and corrected for independently in a parallel manner. As previously discussed, image-based wavefront sensing already provides us with the information for correctly applying different corrections to different parts of the field of view. The drawback, however, was that sequentially correcting for aberrations in different parts of the field of view and digitally recombining a single corrected image reduce the time resolution of the microscope system. In multi-pupil adaptive optics, different parts of the field of view correspond to different orthogonal pupil planes of the microscope system. This was achieved by placing a custom-designed prism arrays to conjugate image planes and add different amounts of angular tilt to the light field as it propagated to different locations in the field of view. From the Fourier shift theorem, the angular tilt induces a spatial shift of the wavefront in the pupil plane. By placing these shifted pupil planes side by side in the form of a two-dimensional tile, a single wavefront modulator can be used to correct for different parts of the field of view both independently and simultaneously. Before the light field enters the back-pupil plane of the objective lens, a compensating prism with opposite tilt angles

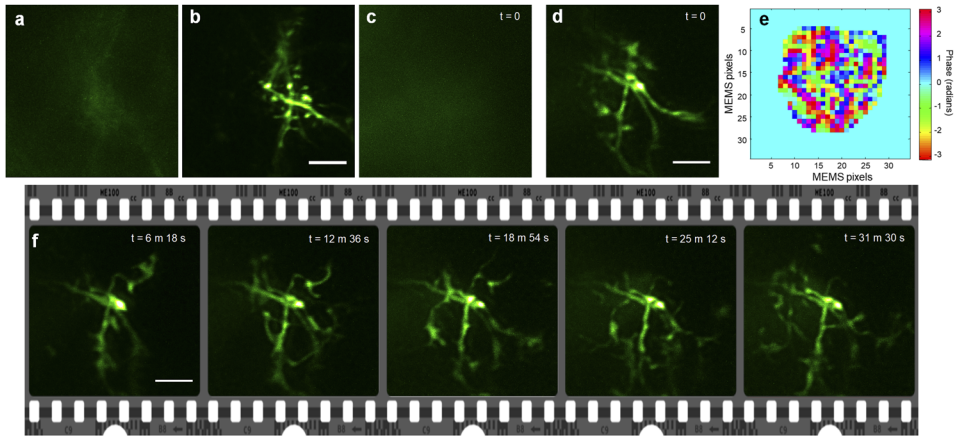

FIG. 4. Imaging through the skull using indirect wavefront sensing. Neuron imaging through the skull with (a) conventional two-photon and (b) wavefront shaped two-photon microscopy. Microglia imaging through the skull with (c) conventional two-photon and (d) wavefront shaped two-photon microscopy. (e) Wavefront correction applied to (d). (f) Time-lapse images of spontaneous neuron activity through the skull of a live mouse. The scale bar is 5 μm. Reproduced with permission from Park *et al.*, Proc. Natl. Acad. Sci. U. S. A. **112**(30), 9236–9241 (2015). Copyright 2015 National Academy of Sciences.

cancels the initial angular tilt, which allows all of the light to enter the objective lens without any loss in throughput. Using this approach, although a single wavefront modulator at the pupil plane is used to control the wavefront of multiple pupils, the entire numerical aperture of the objective lens can be utilized by adjusting the relative magnification factor between the SLM and the objective back-pupil plane.

E. Imaging through dynamic tissues

Until now, the majority of research applying wavefront shaping for *in vivo* studies has focused on two different regimes: (1) relatively transparent systems where the wavefront can be directly measured quickly enough to correct for dynamic aberrations (e.g., retinal systems) and (2) turbid systems where aberrations are more severe, but the corrected aberrations are found to be stable for extended periods of time (e.g., head-fixed mouse brain or immobilized tissue). Dynamic wavefront correction is currently limited to situations where SHWS functions optimally. The ultimate goal, of course, would be to realize dynamic correction for a highly turbid tissue. The difficulty here arises because SHWS fails to operate in such turbid systems.

Since all indirect wavefront measurement schemes developed to date require sequential measurements with measurement numbers proportional to the number of modes that are to be corrected, the only way to utilize indirect wavefront sensing for imaging through dynamic tissue is to perform the numerous measurements faster. Along this line, high-speed MEMS deformable mirrors have enabled direct measurement at ~10 kHz refresh rates. This enables sub-second wavefront measurement for up to a thousand modes, which is accurate enough to focus light through highly turbid tissue, such as the brain or the skull. Another related approach utilizes DMDs, which enable binary amplitude control of the wavefront.[23] Using spatial filtering approaches like Lee's method, binary amplitude modulation can be used for analog phase control, which is required for wavefront shaping. DMDs have speeds comparable with MEMS mirrors at a much lower cost but have very low efficiency when used for phase modulation, which currently limits their direct use in deep tissue imaging.

Another option is to go back to direct wavefront sensing, where only a single measurement is required to follow dynamic aberrations. However, since SHWSs do not work, we must return to holographic measurements. The most notable approach in this direction takes advantage of digital phase conjugation,[22,27,69,128] where the phase-conjugated beam can have arbitrarily larger power than the measured signal. This is critical for imaging or light delivery inside deep tissues. As noted, recent results have demonstrated phase conjugation (including wavefront measurement

and correction wavefront playback) under 10 ms using novel approaches, such as binary phase measurement and modulation based on ferroelectric spatial light modulators.[75]

V. OUTLOOK

The field of wavefront shaping is developing with many different techniques being developed along different aspects, as summarized in Fig. 5. However, all of these techniques have a common goal: to provide deeper, faster, and sharper imaging inside live tissues. Although adaptive optics has already shown direct applications in *in vivo* imaging, the systems where previous techniques can be applied have been limited to either dynamic and transparent systems or static and opaque systems. The final goal would be to apply wavefront shaping to dynamic and opaque systems, which will enable deep tissue imaging in any environment. Past research suggests that indirect wavefront sensing works best for opaque systems, while direct wavefront sensing is optimum for dynamic systems. Recent research in wavefront shaping has, on the other hand, demonstrated that direct wavefront sensing such as phase conjugation could work for opaque systems but has only been demonstrated in model phantom systems where the signal of the beacon could be arbitrarily controlled. In real animal systems, it is likely that phase conjugation would also require a long wavefront measurement time due to low signal levels, thus ruining its temporal advantage. To solve this issue, a hybrid system combining indirect and direct wavefront sensing methods can increase the signal level for fast direct wavefront sensing with high fidelity.

Wavefront shaping would also require new methods to enlarge the effective corrected field of view, which will open new avenues for biological studies. Many techniques developed thus far relied on the memory effect[52,129] and demonstrated impressive results. However, these results were demonstrated only in artificial systems where the distance between the scattering media and the image plane could be arbitrarily controlled. However, in real animal systems, the goal is to focus inside the turbid media rather than through it, and we do not have any degree of freedom to control the distance between the scatterer and the target plane. In this case, recent studies have demonstrated that the translational[53] and angular memory effects[55] will both be in play, which has not yet been fully explored. Further utilizations of optical properties can also enable to address existing challenges in *in vivo* imaging. Recently, time-gated measurements of TMs[130] have shown potentials for high-resolution imaging of objects hidden inside the turbid media. Also, the enhancements in the speed and the number of controllable optical modes[71,76] are crucial for realistic *in vivo* applications. New developments regarding the extension of the effective corrected field of view for correction of a single wavefront are expected to revolutionize *in vivo* bioimaging.

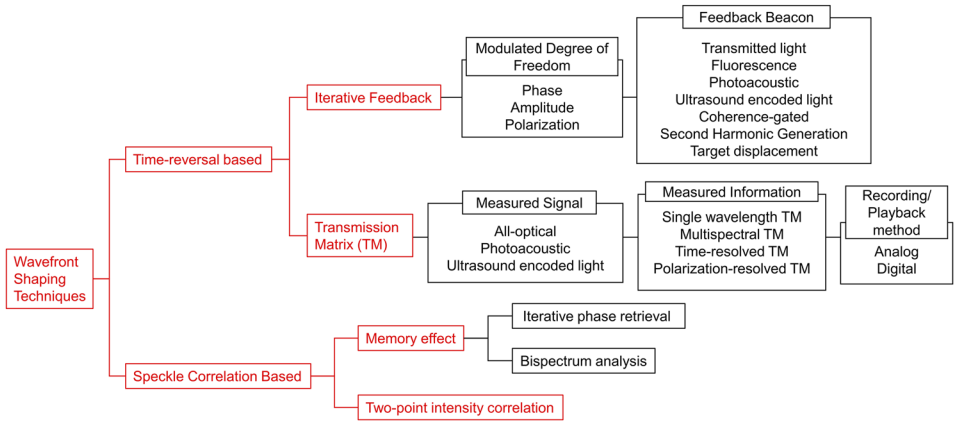

FIG. 5. Current state-of-the-art wavefront shaping techniques utilize various principles. These can be largely divided into two groups: (1) time reversal-based methods and (2) speckle correlation-based methods. Time reversal-based methods either measure the transmission matrix or use iterative feedback using various contrast mechanisms. The speckle correlation-based methods do not actually shape the wavefront, so cannot be used for customized light delivery but rather use speckle correlations to realize non-invasive widefield imaging.

Although this perspective mainly focuses on optical imaging, the wavefront shaping approaches can also be utilized for *in vivo* optical manipulation including optical trapping and optogenetics. Previously, *in situ* wavefront correction was performed through a turbid layer to optically trap spherical particles.[131] It was also shown that complex-shaped biological cells could also be stably trapped and manipulated adaptively shaping the wavefront of a trapping beam.[132] Another interesting application of *in vivo* wavefront shaping would be optogenetics. Recently, the proof of principle toward optical activation and control of cell signaling was demonstrated for optogenetic control of live cells through a mouse skull layer.[133] More recently, focusing on 2-mm-thick living brain tissue and its application in optogenetic modulation of neural activity were demonstrated applying TRUE technique in 800-μm-thick acute mouse brain slices.[96] Going forward, we envision that this generic approach to overcome multiple light scattering in intact biological tissues could have far-reaching applications, not limited to focusing, imaging, and manipulating.

ACKNOWLEDGMENTS

This work was supported by KAIST, BK21+ program, Tomocube, the National Research Foundation of Korea (Nos. 2015R1A3A2066550, 2017M3C1A3013923, 2014K1A3A1A09063027, 2016R1C1B2015130, and 2017M3C7A1044966), the Hong Kong Research Grant Council (No. PolyU 252044/16E), the National Natural Science Foundation of China (Nos. 81671726 and 81627805), and UNIST (No. 1.160050.01).

[1] F. Zernike, Physica **9**(7), 686–698 (1942).
[2] G. Popescu, *Quantitative Phase Imaging of Cells and Tissues* (McGraw Hill Professional, 2011).
[3] K. Lee, K. Kim, J. Jung, J. H. Heo, S. Cho, S. Lee, G. Chang, Y. J. Jo, H. Park, and Y. K. Park, Sensors **13**(4), 4170–4191 (2013).
[4] K. Kim, J. Yoon, S. Shin, S. Lee, S.-A. Yang, and Y. Park, J. Biomed. Photonics Eng. **2**(2), 020201 (2016).
[5] D. Kim, S. Lee, M. Lee, J. Oh, S.-A. Yang, and Y. Park, bioRxiv (2017), p. 106328.
[6] A. Ishimaru, *Wave Propagation and Scattering in Random Media* (Academic Press, New York, 1978).
[7] A. P. Mosk, A. Lagendijk, G. Lerosey, and M. Fink, Nat. Photonics **6**(5), 283–292 (2012).
[8] H. Yu, J. Park, K. Lee, J. Yoon, K. Kim, S. Lee, and Y. Park, Curr. Appl. Phys. **15**(5), 632–641 (2015).
[9] S. M. Popoff, G. Lerosey, R. Carminati, M. Fink, A. C. Boccara, and S. Gigan, Phys. Rev. Lett. **104**(10), 100601 (2010).
[10] J. Park, J.-Y. Cho, C. Park, K. Lee, H. Lee, Y.-H. Cho, and Y. Park, ACS Nano **10**(7), 6871 (2016).
[11] J.-H. Park, C. Park, H. Yu, J. Park, S. Han, J. Shin, S. H. Ko, K. T. Nam, Y.-H. Cho, and Y. Park, Nat. Photonics **7**(6), 454–458 (2013).
[12] J.-H. Park, C. Park, H. Yu, Y.-H. Cho, and Y. Park, Opt. Express **20**(15), 17010–17016 (2012).
[13] J.-H. Park, C. Park, H. Yu, Y.-H. Cho, and Y. Park, Opt. Lett. **37**(15), 3261–3263 (2012).
[14] V. Ntziachristos, Nat. Methods **7**, 603 (2010).
[15] T. J. Farrell, M. S. Patterson, and B. Wilson, Med. Phys. **19**(4), 879–888 (1992).
[16] L. Wang, S. L. Jacques, and L. Zheng, Comput. Methods Programs Biomed. **47**(2), 131–146 (1995).
[17] I. M. Vellekoop and A. P. Mosk, Opt. Lett. **32**(16), 2309–2311 (2007).
[18] S. Popoff, G. Lerosey, M. Fink, A. C. Boccara, and S. Gigan, Nat. Commun. **1**, 81 (2010).
[19] I. M. Vellekoop and A. P. Mosk, Opt. Commun. **281**(11), 3071–3080 (2008).
[20] D. Akbulut, T. J. Huisman, E. G. van Putten, W. L. Vos, and A. P. Mosk, Opt. Express **19**(5), 4017–4029 (2011).
[21] I. M. Vellekoop, Opt. Express **23**(9), 12189–12206 (2015).
[22] M. Cui, E. J. McDowell, and C. Yang, Opt. Express **18**(1), 25–30 (2010).
[23] D. B. Conkey, A. M. Caravaca-Aguirre, and R. Piestun, Opt. Express **20**(2), 1733–1740 (2012).
[24] Z. Yaqoob, D. Psaltis, M. S. Feld, and C. Yang, Nat. Photonics **2**(2), 110–115 (2008).
[25] T. R. Hillman, T. Yamauchi, W. Choi, R. R. Dasari, M. S. Feld, Y. Park, and Z. Yaqoob, Sci. Rep. **3**, 1909 (2013).
[26] K. Lee, J. Lee, J.-H. Park, J.-H. Park, and Y. Park, Phys. Rev. Lett. **115**(15), 153902 (2015).
[27] M. Cui and C. Yang, Opt. Express **18**(4), 3444–3455 (2010).
[28] R. Horstmeyer, H. Ruan, and C. Yang, Nat. Photonics **9**, 563 (2015).
[29] M. Cui, Opt. Lett. **36**(6), 870–872 (2011).
[30] J. Yoon, K. Lee, J. Park, and Y. Park, Opt. Express **23**(8), 10158–10167 (2015).
[31] W. Harm, C. Roider, A. Jesacher, S. Bernet, and M. Ritsch-Marte, Opt. Express **22**(18), 22146–22156 (2014).
[32] A. K. Singh, D. N. Naik, G. Pedrini, M. Takeda, and W. Osten, Opt. Express **22**(7), 7694–7701 (2014).
[33] H. Yu, Y. Baek, J. Park, S. Han, K. Lee, and Y. Park, ITE Trans. Media Technol. Appl. **5**(3), 78–87 (2017).
[34] A. K. Singh, D. N. Naik, G. Pedrini, M. Takeda, and W. Osten, Light: Sci. Appl. **6**(2), e16219 (2017).
[35] S. Popoff, G. Lerosey, R. Carminati, M. Fink, A. Boccara, and S. Gigan, Phys. Rev. Lett. **104**(10), 100601 (2010).
[36] H. Yu, T. R. Hillman, W. Choi, J. O. Lee, M. S. Feld, R. R. Dasari, and Y. Park, Phys. Rev. Lett. **111**(15), 153902 (2013).
[37] K. Lee and Y. Park, Nat. Commun. **7**, 13359 (2016).
[38] Y. Baek, K. Lee, and Y. Park, preprint arXiv:1802.10321 (2018).
[39] I. N. Papadopoulos, S. Farahi, C. Moser, and D. Psaltis, Biomed. Opt. Express **4**(2), 260–270 (2013).
[40] T. Čižmár and K. Dholakia, Nat. Commun. **3**, 1027 (2012).

[41] Y. Choi, C. Yoon, M. Kim, T. D. Yang, C. Fang-Yen, R. R. Dasari, K. J. Lee, and W. Choi, Phys. Rev. Lett. **109**(20), 203901 (2012).
[42] I. M. Vellekoop, E. G. van Putten, A. Lagendijk, and A. P. Mosk, Opt. Express **16**(1), 67–80 (2008).
[43] B. Judkewitz, Y. M. Wang, R. Horstmeyer, A. Mathy, and C. Yang, Nat. Photonics **7**(4), 300–305 (2013).
[44] H. Ruan, M. Jang, and C. Yang, Nat. Commun. **6**, 8968 (2015).
[45] I. Freund, M. Rosenbluh, and S. Feng, Phys. Rev. Lett. **61**(20), 2328–2331 (1988).
[46] S. Feng, C. Kane, P. A. Lee, and A. D. Stone, Phys. Rev. Lett. **61**(7), 834–837 (1988).
[47] O. Katz, E. Small, and Y. Silberberg, Nat. Photonics **6**, 549 (2012).
[48] I. M. Vellekoop and C. M. Aegerter, Opt. Lett. **35**(8), 1245–1247 (2010).
[49] J. Bertolotti, E. G. van Putten, C. Blum, A. Lagendijk, W. L. Vos, and A. P. Mosk, Nature **491**, 232 (2012).
[50] J. Tang, R. N. Germain, and M. Cui, Proc. Natl. Acad. Sci. U. S. A. **109**(22), 8434–8439 (2012).
[51] O. Katz, P. Heidmann, M. Fink, and S. Gigan, Nat. Photonics **8**, 784 (2014).
[52] X. Yang, Y. Pu, and D. Psaltis, Opt. Express **22**(3), 3405–3413 (2014).
[53] B. Judkewitz, R. Horstmeyer, I. M. Vellekoop, I. N. Papadopoulos, and C. Yang, Nat. Phys. **11**, 684 (2015).
[54] G. Osnabrugge, R. Horstmeyer, I. N. Papadopoulos, B. Judkewitz, and I. M. Vellekoop, Optica **4**(8), 886–892 (2017).
[55] S. Schott, J. Bertolotti, J.-F. Léger, L. Bourdieu, and S. Gigan, Opt. Express **23**(10), 13505–13516 (2015).
[56] R. Kumar Singh and M. Anandraj Sharma, Appl. Phys. Lett. **104**(11), 111108 (2014).
[57] A. S. Somkuwar, B. Das, R. Vinu, Y. Park, and R. K. Singh, J. Opt. Soc. Am. A **34**(8), 1392–1399 (2017).
[58] D. B. Conkey, A. N. Brown, A. M. Caravaca-Aguirre, and R. Piestun, Opt. Express **20**(5), 4840–4849 (2012).
[59] T. Chaigne, O. Katz, A. C. Boccara, M. Fink, E. Bossy, and S. Gigan, Nat. Photonics **8**(1), 58–64 (2014).
[60] E. Bossy and S. Gigan, Photoacoustics **4**(1), 22–35 (2016).
[61] Z. Yu, H. Li, and P. Lai, Appl. Sci. **7**(12), 1320 (2017).
[62] J. Aulbach, B. Gjonaj, P. M. Johnson, A. P. Mosk, and A. Lagendijk, Phys. Rev. Lett. **106**(10), 103901 (2011).
[63] S. Rotter and S. Gigan, Rev. Mod. Phys. **89**(1), 015005 (2017).
[64] P. Lai, X. Xu, H. Liu, Y. Suzuki, and L. V. Wang, J. Biomed. Opt. **16**(8), 080505 (2011).
[65] H. Liu, X. Xu, P. Lai, and L. V. Wang, J. Biomed. Opt. **16**(8), 086009 (2011).
[66] P. Lai, X. Xu, H. Liu, and L. V. Wang, J. Biomed. Opt. **17**(3), 030506-1–030506-3 (2012).
[67] Y. Liu, P. Lai, C. Ma, X. Xu, A. A. Grabar, and L. V. Wang, Nat. Commun. **6**, 5904 (2015).
[68] Y. Shen, Y. Liu, C. Ma, and L. V. Wang, Optica **4**(1), 97–102 (2017).
[69] Y. Shen, Y. Liu, C. Ma, and L. V. Wang, J. Biomed. Opt. **21**(8), 085001 (2016).
[70] P. Lai, L. Wang, J. W. Tay, and L. V. Wang, Nat. Photonics **9**(2), 126–132 (2015).
[71] H. Yu, K. Lee, and Y. Park, Opt. Express **25**(7), 8036–8047 (2017).
[72] K. Si, R. Fiolka, and M. Cui, Nat. Photonics **6**(10), 657–661 (2012).
[73] I. M. Vellekoop, M. Cui, and C. Yang, Appl. Phys. Lett. **101**(8), 081108 (2012).
[74] M. Jang, H. Ruan, H. Zhou, B. Judkewitz, and C. Yang, Opt. Express **22**(12), 14054–14071 (2014).
[75] Y. Liu, C. Ma, Y. Shen, J. Shi, and L. V. Wang, Optica **4**(2), 280–288 (2017).
[76] D. Wang, E. H. Zhou, J. Brake, H. Ruan, M. Jang, and C. Yang, Optica **2**(8), 728–735 (2015).
[77] J. W. Tay, P. X. Lai, Y. Suzuki, and L. V. Wang, Sci. Rep. **4**, 3918 (2014).
[78] I. M. Vellekoop and A. Mosk, Phys. Rev. Lett. **101**(12), 120601 (2008).
[79] J. V. Thompson, G. A. Throckmorton, B. H. Hokr, and V. V. Yakovlev, Opt. Lett. **41**(8), 1769–1772 (2016).
[80] Y. M. Wang, B. Judkewitz, C. A. DiMarzio, and C. Yang, Nat. Commun. **3**, 928 (2012).
[81] X. Xu, H. Liu, and L. V. Wang, Nat. Photonics **5**(3), 154–157 (2011).
[82] E. H. Zhou, H. Ruan, C. Yang, and B. Judkewitz, Optica **1**(4), 227–232 (2014).
[83] C. Ma, X. Xu, Y. Liu, and L. V. Wang, Nat. Photonics **8**(12), 931–936 (2014).
[84] Z. Yu, J. Huangfu, F. Zhao, M. Xia, X. Wu, X. Niu, D. Li, P. Lai, and D. Wang, Sci. Rep. **8**(1), 2927 (2018).
[85] H. Ruan, T. Haber, Y. Liu, J. Brake, J. Kim, J. M. Berlin, and C. Yang, Optica **4**(11), 1337–1343 (2017).
[86] F. Kong, R. H. Silverman, L. Liu, P. V. Chitnis, K. K. Lee, and Y.-C. Chen, Opt. Lett. **36**(11), 2053–2055 (2011).
[87] A. M. Caravaca-Aguirre, D. B. Conkey, J. D. Dove, H. Ju, T. W. Murray, and R. Piestun, Opt. Express **21**(22), 26671–26676 (2013).
[88] T. Chaigne, J. Gateau, O. Katz, C. Boccara, S. Gigan, and E. Bossy, Opt. Lett. **39**(20), 6054–6057 (2014).
[89] X. L. Deán-Ben, H. Estrada, and D. Razansky, Opt. Lett. **40**(4), 443–446 (2015).
[90] J. W. Tay, J. Liang, and L. V. Wang, Opt. Lett. **39**(19), 5499–5502 (2014).
[91] D. B. Conkey, A. M. Caravaca-Aguirre, J. D. Dove, H. Y. Ju, T. W. Murray, and R. Piestun, Nat. Commun. **6**, 7902 (2015).
[92] L. V. Wang and S. Hu, Science **335**(6075), 1458–1462 (2012).
[93] L. V. Wang and H.-i. Wu, *Biomedical Optics: Principles and Imaging* (John Wiley & Sons, 2012).
[94] L. Wang, C. Zhang, and L. V. Wang, Phys. Rev. Lett. **113**(17), 174301 (2014).
[95] P. Lai, Y. Suzuki, X. Xu, and L. V. Wang, Laser Phys. Lett. **10**(7), 075604 (2013).
[96] H. Ruan, J. Brake, J. E. Robinson, Y. Liu, M. Jang, C. Xiao, C. Zhou, V. Gradinaru, and C. Yang, Sci. Adv. **3**(12), eaao5520 (2017).
[97] J. W. Hardy, *Adaptive Optics for Astronomical Telescopes* (Oxford University Press on Demand, 1998).
[98] H. W. Babcock, Publ. Astron. Soc. Pac. **65**(386), 229–236 (1953).
[99] M. J. Booth, Light: Sci. Appl. **3**(4), e165 (2014).
[100] M. J. Booth, Philos. Trans. R. Soc., A **365**(1861), 2829–2843 (2007).
[101] J. A. Kubby, *Adaptive Optics for Biological Imaging* (CRC Press, 2013).
[102] X. Tao, J. Crest, S. Kotadia, O. Azucena, D. C. Chen, W. Sullivan, and J. Kubby, Opt. Express **20**(14), 15969–15982 (2012).
[103] A. Roorda, F. Romero-Borja, W. J. Donnelly III, H. Queener, T. J. Hebert, and M. C. Campbell, Opt. Express **10**(9), 405–412 (2002).

[104] K. Wang, D. E. Milkie, A. Saxena, P. Engerer, T. Misgeld, M. E. Bronner, J. Mumm, and E. Betzig, Nat. Methods **11**(6), 625–628 (2014).
[105] A. Roorda and D. R. Williams, Nature **397**(6719), 520–522 (1999).
[106] Y. Zhang and A. Roorda, J. Biomed. Opt. **11**(1), 014002–014005 (2006).
[107] S. Tuohy and A. G. Podoleanu, Opt. Express **18**(4), 3458–3476 (2010).
[108] J. Wang, J.-F. Léger, J. Binding, A. C. Boccara, S. Gigan, and L. Bourdieu, Biomed. Opt. Express **3**(10), 2510–2525 (2012).
[109] M. Rueckel, J. A. Mack-Bucher, and W. Denk, Proc. Natl. Acad. Sci. U. S. A. **103**(46), 17137–17142 (2006).
[110] M. J. Booth, M. A. Neil, R. Juškaitis, and T. Wilson, Proc. Natl. Acad. Sci. U. S. A. **99**(9), 5788–5792 (2002).
[111] N. Ji, D. E. Milkie, and E. Betzig, Nat. Methods **7**(2), 141–147 (2010).
[112] R. K. Tyson, *Principles of Adaptive Optics* (CRC Press, 2015).
[113] R. Aviles-Espinosa, J. Andilla, R. Porcar-Guezenec, O. E. Olarte, M. Nieto, X. Levecq, D. Artigas, and P. Loza-Alvarez, Biomed. Opt. Express **2**(11), 3135–3149 (2011).
[114] P. Marsh, D. Burns, and J. Girkin, Opt. Express **11**(10), 1123–1130 (2003).
[115] L. Kong and M. Cui, Opt. Express **22**(20), 23786–23794 (2014).
[116] D. Débarre, E. J. Botcherby, T. Watanabe, S. Srinivas, M. J. Booth, and T. Wilson, Opt. Lett. **34**(16), 2495–2497 (2009).
[117] R. Fiolka, K. Si, and M. Cui, Opt. Express **20**(15), 16532–16543 (2012).
[118] J. Jang, J. Lim, H. Yu, H. Choi, J. Ha, J.-H. Park, W.-Y. Oh, W. Jang, S. Lee, and Y. Park, Opt. Express **21**(3), 2890–2902 (2013).
[119] H. Yu, J. Jang, J. Lim, J.-H. Park, W. Jang, J.-Y. Kim, and Y. Park, Opt. Express **22**(7), 7514–7523 (2014).
[120] H. Yu, P. Lee, K. Lee, J. Jang, J. Lim, W. Jang, Y. Jeong, and Y. Park, J. Biomed. Opt. **21**(10), 101406 (2016).
[121] R. Ragazzoni, E. Marchetti, and G. Valente, Nature **403**(6765), 54 (2000).
[122] J. Mertz, H. Paudel, and T. G. Bifano, Appl. Opt. **54**(11), 3498–3506 (2015).
[123] T.-w. Wu and M. Cui, Opt. Express **23**(6), 7463–7470 (2015).
[124] Z. Kam, P. Kner, D. Agard, and J. W. Sedat, J. Microsc. **226**(1), 33–42 (2007).
[125] J. Thaung, P. Knutsson, Z. Popovic, and M. Owner-Petersen, Opt. Express **17**(6), 4454–4467 (2009).
[126] J.-H. Park, W. Sun, and M. Cui, Proc. Natl. Acad. Sci. U. S. A. **112**(30), 9236–9241 (2015).
[127] J.-H. Park, L. Kong, Y. Zhou, and M. Cui, Nat. Methods **14**(6), 581 (2017).
[128] M. Jang, H. Ruan, I. M. Vellekoop, B. Judkewitz, E. Chung, and C. Yang, Biomed. Opt. Express **6**(1), 72–85 (2015).
[129] C.-L. Hsieh, Y. Pu, R. Grange, G. Laporte, and D. Psaltis, Opt. Express **18**(20), 20723–20731 (2010).
[130] S. Jeong, Y.-R. Lee, W. Choi, S. Kang, J. H. Hong, J.-S. Park, Y.-S. Lim, H.-G. Park, and W. Choi, Nat. Photonics **12**, 277 (2018).
[131] T. Čižmár, M. Mazilu, and K. Dholakia, Nat. Photonics **4**(6), 388 (2010).
[132] K. Kim and Y. Park, Nat. Commun. **8**, 15340 (2017).
[133] J. Yoon, M. Lee, K. Lee, N. Kim, J. M. Kim, J. Park, H. Yu, C. Choi, W. Do Heo, and Y. Park, Sci. Rep. **5**, 13289 (2015).